Measuring Freeze and Thaw Damage in Mortars Containing Deicing Salt Using a Low Temperature Longitudinal Guarded Comparative Calorimeter and Acoustic Emission (AE-LGCC)

Article *in* Advances in Civil Engineering Materials · July 2014

DOI: 10.1520/ACEM20130095

CITATIONS
85

READS
4,989

5 authors, including:

Yaghoob Amir Farnam
Drexel University
72 PUBLICATIONS **2,130** CITATIONS
SEE PROFILE

D. P. Bentz
National Institute of Standards and Technology
398 PUBLICATIONS **21,681** CITATIONS
SEE PROFILE

Aaron Richard Sakulich
Worcester Polytechnic Institute
44 PUBLICATIONS **1,776** CITATIONS
SEE PROFILE

William Jason Weiss
Oregon State University
560 PUBLICATIONS **16,832** CITATIONS
SEE PROFILE

Advances in Civil Engineering Materials, 3 (1), 23 pp., 2014.

Measuring Freeze and Thaw Damage in Mortars Containing Deicing Salt Using a Low Temperature Longitudinal Guarded Comparative Calorimeter and Acoustic Emission (AE-LGCC)

Yaghoob Farnam[(1)], Dale Bentz[(2)], Aaron Sakulich[(3)], Daniel Flynn[(4)], and Jason Weiss[(5)]

[(1)] Graduate Research Assistant, Ph.D. Student, School of Civil Engineering, Purdue University, 550 Stadium Mall Dr., West Lafayette, IN 47907, USA, yfarnam@purdue.edu

[(2)] Chemical Engineer, Materials and Structural Systems Division, National Institute of Standards and Technology, 100 Bureau Drive, Stop 8615, Gaithersburg, MD 20899, USA, dale.bentz@nist.gov

[(3)] Assistant Professor, Department of Civil and Environmental Engineering, Worcester Polytechnic Institute, 100 Institute Road, Worcester, MA 01609, USA, arsakulich@wpi.edu

[(4)] Research Associate, Energy and Environment Division, National Institute of Standards and Technology, 100 Bureau Drive, Stop 8615, Gaithersburg, MD 20899, USA, daniel.flynn@nist.gov

[(5)] Professor, Director of Pankow Materials Laboratory, School of Civil Engineering, Purdue University, 550 Stadium Mall Dr., West Lafayette, IN 47907, wjweiss@purdue.edu

ABSTRACT

Deicing salts are often applied to the surface of pavements and bridge decks in the winter to melt ice; thereby improving safety for the travelling public. In this paper, the influence of NaCl deicing salt on freezing and thawing temperatures of pore solution and corresponding damage of mortar specimens were investigated. A low-temperature longitudinal guarded comparative calorimeter (LGCC) was developed to cool down a mortar sample at a rate of 2 °C/h and to re-heat the mortar at a rate of 4 °C/h. Heat flux during freezing and thawing cycles was monitored, and the temperatures at which freezing and thawing events occurred were detected. During cooling and heating, acoustic emission activity was measured to quantify the damage (cracking) due to aggregate/paste thermal mismatch and/or phase changes. The results show that NaCl solution in a mortar sample freezes at a lower temperature than the value expected from its bulk phase diagram due to under-cooling. Conversely, the frozen solution in mortar melts at the same melting temperature as the bulk frozen NaCl solution. As the salt concentration increases, the freezing temperature is lowered. For samples containing more highly concentrated solutions, an additional exothermic event is observed whose corresponding temperature is greater than the aqueous NaCl liquidus line in the phase diagram. Damage also begins to occur at this temperature. For mortar samples saturated by solutions with 5 % and 15 % NaCl by mass, greater freeze/thaw damage is observed. The AE calorimeter developed herein is applicable for investigating damage behavior during freezing and thawing of different phases in pore solution (in mortars).

Keywords: Acoustic Emission, Calorimeter, Concrete, Deicing Salts, Freeze and Thaw, Heat Flow, Mortar, NaCl.

1.0 Introduction

Concrete can be damaged when first, it is sufficiently wet (has a high degree of saturation) and second, it experiences temperature cycles that enable freezing and thawing. The damage that occurs due to freezing and thawing can lead to premature deterioration, costly repairs, and early replacement of concrete infrastructure elements. In cold climates, when the degree of saturation exceeds 86 % to 88 % [1], freeze-thaw damage is inevitable, even after only a few freeze/thaw cycles. To reduce this freeze/thaw damage, engineered air voids (e.g., air entrainment) can be considered in mixture proportioning [2].

Deicing salt is used to depress the freezing point of the water on the concrete surface. Although addition of deicing salts on the surface of concrete elements can melt the ice and increase the safety of infrastructure. The molten salty solution can be absorbed into concrete pores and can also cause severe damage to concrete structures by inducing corrosion of reinforcing steel (as many deicing salts contain chlorides), scaling of the concrete, or salt crystallization which causes damage to the concrete.

1.1 Mechanisms of freeze and thaw damage in Concrete

During freeze/thaw deterioration of concrete exposed to deicing salt, a variety of complex damage mechanisms occur [2–9]. First, the formation of ice inside the concrete pore structure produces hydraulic pressure [3]. Recognition of the role of hydraulic pressure in freeze/thaw damage led to the initial introduction of air voids into concrete [2]. In addition to hydraulic pressure caused by 9 % volume expansion of water freezing in large cavities, the osmotic pressure resulting from partial freezing of solutions in capillaries can be another source of deterioration in concrete [4]. In fact, the difference in solution concentration between partially frozen solution in larger pores and unfrozen solution in smaller pores causes the transport of water from smaller pores to larger pores causing an additional pressure (i.e., osmotic pressure). Another form of destructive expansion was observed by Beaudoin and McInnis [5] where expansion of the cement paste occurred when the cement paste pore structure was saturated by benzene instead of water, which contracts upon freezing. Another hypothesis in frost damage described by Litvan [6] was large-scale migration of unfrozen water from small pores (high entropy region)

to large cavities filled by frozen water (low entropy region). In fact, the difference in energies in the two regions causes large-scale migration which could produce further expansion and more damage.

In addition, when ice crystals form in pores, stresses are generated by their crystallization that depend on pore size, the energy of the interface between the pore wall and the crystal, and the yield stress of the crystal [7]. An increasing concentration of salt produces a greater depression of the freezing point; however, crystallization of salt may occur inside the pores. The pressure caused by salt crystallization is strong enough to cause severe damage in concrete [8,9].

Most of the hypotheses that have been introduced to explain freeze/thaw damage are only partially validated; more research needs to be performed to understand the role of deicing salt in the damage mechanisms of paste, mortar, and concrete. To do so, powerful experimental techniques are required to detect and define the damage mechanisms caused by different components inside a porous cementitious material exposed to deicing salt. This can be done by either heat flow analysis of phase changes in pore solution or acoustic emission detection of microcrack and crack formation. Therefore, these two techniques are combined into a single experimental setup in the present paper.

1.2 Background on Heat Transitions of Liquid/Solid Phase Changes in Concrete Pore Solution

Pure water freezes at 0 °C at atmospheric pressure. However, water inside concrete pores is not pure, as it contains several soluble species such as various alkalis, chloride, and hydroxide. The presence of ions in pore solution causes that pore solution to freeze at a temperature lower than what is expected of pure water [9]. In addition, a further decrease of the freezing point of pore solution in porous materials occurs due to surface interactions, confinement, and the presence of capillary pressures [7,10].

In cold climates, when deicing salts are added to the surface of pavements and bridge decks, the ions concentration in the pore solution is increased. In general, using more salt produces a higher concentration of ions in pores and leads to greater depression of the freezing point. Fig. 1 shows a phase diagram of aqueous NaCl. In this phase diagram, four phases exist including aqueous NaCl solution, ice, NaCl, and $NaCl{\cdot}2H_2O$ (hydrohalite). When one phase transforms to another phase, latent heat must either be released or absorbed. Therefore, energy is transferred, which can indicate that a freezing or

thawing phase change is occurring [6,11]. The amount of latent heat and its corresponding freezing or thawing temperatures are specific material properties that can be used to differentiate different materials and different phases in a composite system.

Low temperature heat flow studies of porous cementitious materials have conventionally been performed on very small cement paste samples [6,10,12]. Low temperature differential scanning calorimeters have been often used to investigate phase transformations of water and NaCl solution in hardened cement paste. The low temperature calorimeter has been also used to define the freezing and thawing behavior of small mortar samples [13,14]. Despite the ability of these techniques to accurately measure heat flows of different phase transitions, the small size of samples prohibits the testing of composite systems containing fine and coarse aggregates. A longitudinal guarded comparative heat flow technique [15] is often used to quantify the heat flow and thermal properties of composites, and could be applied for mortar and concrete samples. In this research, this heat flow technique is used to quantify the heat flow in mortar samples. It is anticipated that this can be extended to concrete samples.

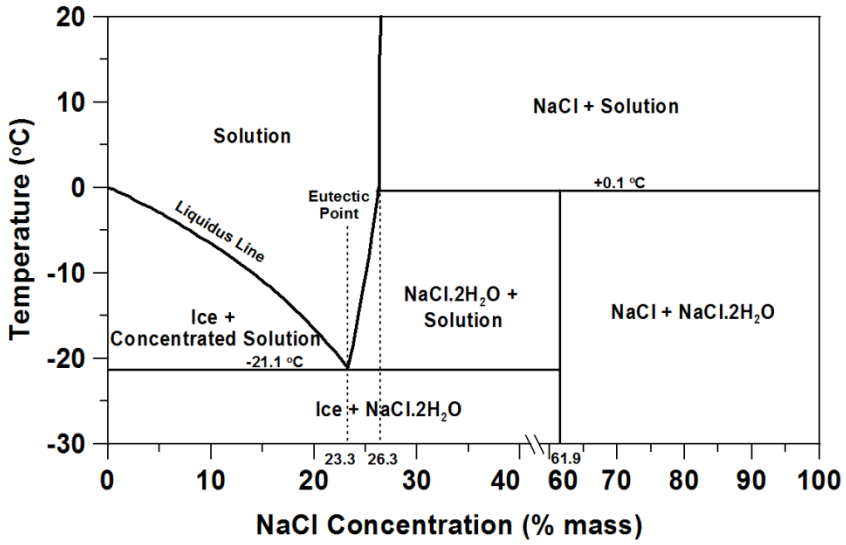

Fig. 1— Phase diagram of aqueous NaCl.

1.3 Background on Use of Acoustic Emission (AE) to Quantify Freeze-Thaw Damage

Different acoustic emission (AE) techniques are conventionally employed to quantify the damage in concrete caused by destructive phenomena [16–19]. They can also be used to detect damage caused by freeze/thaw cycles in concrete [1,20–26]. A resonant frequency technique or a pulse/wave velocity technique can be used to quantify the extent of damage in concrete samples exposed to freezing and thawing [20–23]. The main drawback of the resonant frequency and the pulse/wave velocity techniques is that they are conventionally limited to discrete measurements of bulk sample deterioration. In other words, continuous measurement is almost impossible using these techniques and they give almost no information about the moment at which micro/macro cracks are generated, and whether they are generated within paste, aggregate, or interfacial transition zones. In an advanced method, a passive acoustic emission technique is used alongside an active or pulse velocity technique to understand the behavior of concrete cracking during freezing and thawing [1,8,24–26].

1.4 Research Significance

Most of the hypotheses described for freeze/thaw damage are only partially validated and more investigations are required. In addition, a testing technique which can detect both damage and heat flow during liquid/solid phase changes inside a composite pore structure is not readily available. When deicers (such as NaCl) are used to depress freezing points, complex damage phenomena may occur that cannot be described by existing experimental devices.

The main objectives of this study are: first, to develop an experimental technique that can characterize freeze/thaw damage action; second, to determine and correlate damage and phase change events by monitoring the acoustic and thermal behavior of mortar samples containing NaCl solution; and third, to detect how NaCl influences the damage mechanisms, freezing temperature, and melting temperature of different phases in saturated mortar samples.

2.0 Experimental Program

2.1 Materials and mixture proportioning

Ordinary Type I portland cement (OPC) with a fineness of 375 m^2/kg was used in this study. The chemical composition of this cement is indicated in Table 1. Aggregates used in this study consisted of natural sand with a maximum size of 4.75 mm, specific gravity of 2.61, and an absorption value of 2.2 % by mass. A single mortar mixture was used with a sand volume fraction of 55 % and a water-to-cement ratio (*w/c*) of 0.42 by mass. No chemical admixtures or supplementary cementitious materials were used. Mixture proportioning for making the mortar samples is shown in Table 2.

Table 1—Properties of Type I ordinary portland cement (OPC).

Item	Percent by mass (%)
Silicon Dioxide (SiO_2)	19.43
Aluminum Oxide (Al_2O_3)	5.39
Ferric Oxide (Fe_2O_3)	3.18
Calcium Oxide (CaO)	63.45
Magnesium Oxide (MgO)	2.97
Sulfur Trioxide (SO_3)	3.38
Loss on Ignition	0.88
Sodium Oxide	0.35
Potassium Oxide	0.77
Insoluble Residue	0.25
Total Equivalent Alkali as Na_2O	0.86
Tricalcium Silicate (C_3S)	60
Dicalcium Silicate (C_2S)	10
Tricalcium Aluminate (C_3A)	9
Tetracalcium Aluminoferrite (C_4AF)	10

Table 2—Mixture proportions of mortar (Saturated-Surface-Dry)

Item	Type	Unit	Amount
Cement	Type I	kg/m^3	612
Aggregate	Sand (0-4.75mm)	kg/m^3	1435
Water	-	kg/m^3	257
w/c	-	Ratio by mass	0.42

2.2 Sample Preparation and Conditioning

The mortar was prepared in a standard mortar mixer in accordance with ASTM C305-12 [27]. The cement was mixed with water for 30 s at the low speed. Sand was then slowly added to the mixer within 30 s, while the mixture was being mixed at the low speed. The entire mixture was mixed for another 30 s at medium speed. The mixing was stopped for 90 s as the sides and bottom of the mixing bowl were scraped. A final 90 s of mixing was at medium speed. The mortar was cast in 25.4 mm × 25.4 mm × 300 mm (1 in × 1 in × 11.81 in) molds that were demolded after 24 h. All mortar bars were then sealed in double plastic bags and cured for 28 d in these sealed conditions at 23 °C ± 0.5 °C. After 28 d of curing, the mortar bars were cut using a wet saw to 25.4 mm × 25.4 mm × 50.8 mm (1 in × 1 in × 2 in) samples. Samples were then placed in a vacuum oven at 65 °C ± 1 °C and a pressure of 20 mm Hg ± 5 mm Hg for 7 d. The ± 1 °C and ± 5 mm Hg are indicative of the nominal operating range encountered when running the experiment.

The samples were then placed in a desiccator using two small spacers underneath each sample to provide a small gap between the bottom of the container and the lower surface of sample. The samples were evacuated to a pressure of 10 mm Hg ± 5 mm Hg for 3.5 h. After evacuation and while still under vacuum, de-aerated NaCl solution (de-aerated by vacuuming the solution for 15 min) was introduced into the desiccator to cover the samples for 1 h. Soaked samples inside NaCl solution were transferred to a 23 °C ± 0.5 °C chamber before testing, where they were kept in a beaker for 3 d. This condition was considered as fully saturated (i.e., assuming 100 % degree of saturation).

After conditioning, samples were wrapped with a thin plastic sheet to protect the samples against subsequent moisture exchange with their surrounding environment (preventing them from absorbing or releasing water during the freeze-thaw process). The top and bottom cross section plastic covers were removed to ensure better connection with thermal pads during the freeze/ thaw tests. In addition, a small circular hole was made in the side plastic of each sample to attach the AE sensor.

3.0 Testing Design and Procedure

Different samples were prepared for freeze/thaw testing. Samples were saturated by different NaCl solutions. Pure salt and de-ionized water were used to prepare NaCl solutions with (0, 0.7, 3, 5, 6, 8, 10, 13, 15, 18, 23.3, and 26) % NaCl by mass. Dry control samples were also prepared for comparative testing.

3.1 Low Temperature Longitudinal Guarded Comparative Calorimeter (LGCC)

During solid/liquid phase changes, a large amount of heat is released or absorbed. The amount and rate of this heat exchange is an indication of different components and their volume fractions within a system. Under steady state thermal conditions, the heat flow of a material can be measured by means of the longitudinal guarded comparative heat flow technique [15,28]. In this technique, one-dimensional heat flow is produced by using a heat sink and a longitudinal guarded (insulated) shell. Two samples of known thermal properties are used as meter bars to comparatively measure the heat flow through a sample with unknown thermal properties.

In this study, a LGCC was constructed according to ASTM E1225-09 [15] and ASTM D5470-12 [28] to produce and to quantify heat flow. A test sample was inserted between two 25.4 mm × 25.4 mm × 25.4 mm (1 in × 1 in × 1 in) meter bars with known thermal properties. In this study, Pyroceram Code 9606 material[1] was used as the meter bar material. The thermal conductivity of this material as a function of temperature can be calculated by Eq. 1 [29]:

$$\lambda_{PC} = -0.0061(T) + 4.2013 \qquad -50\,°C < T < 30\,°C \qquad (1)$$

where λ_{PC} is the thermal conductivity of the Pyroceram (W/(m·K)) and T is its temperature (°C).

A temperature gradient was established in the test sample by using a two stage cold plate (Cascade CCP-22[1] [30]) as shown in Figs. 2a and 2b. The two stage cold plate is capable of decreasing the temperature to as low as -58 °C in a 25 °C ambient temperature environment. To establish one-

[1] Certain commercial products are identified in this paper to specify the materials used and procedures employed. In no case does such identification imply endorsement or recommendation by the National Institute of Standards and Technology, or Purdue University, nor does it indicate that the products are necessarily the best available for the purpose.

dimensional heat flow, heat losses in lateral directions were minimized by using a longitudinal guard having approximately the same temperature gradient. In addition, thermal insulation was placed between the longitudinal guard and the sample. Insulation was also placed in the environment surrounding the longitudinal guard to further prevent heat losses (Fig. 2).

Thermally conductive pads (ThermaCool TC3008[1]) with a thickness of 3 mm, thermal conductivity of 3.0 W/(m·K), and an operating temperature range of -55 °C to 200 °C were used at the Pyroceram/mortar sample and Pyroceram/cold plate interfaces. Seven thermocouples with an accuracy of ± 0.1 °C were positioned at different heights (Fig. 2c) to measure corresponding temperatures and heat flow through the LGCC. It should be noted that the heat flow measured by this technique is an approximate measurement, since the designed LGCC is operating under quasi-steady state conditions.

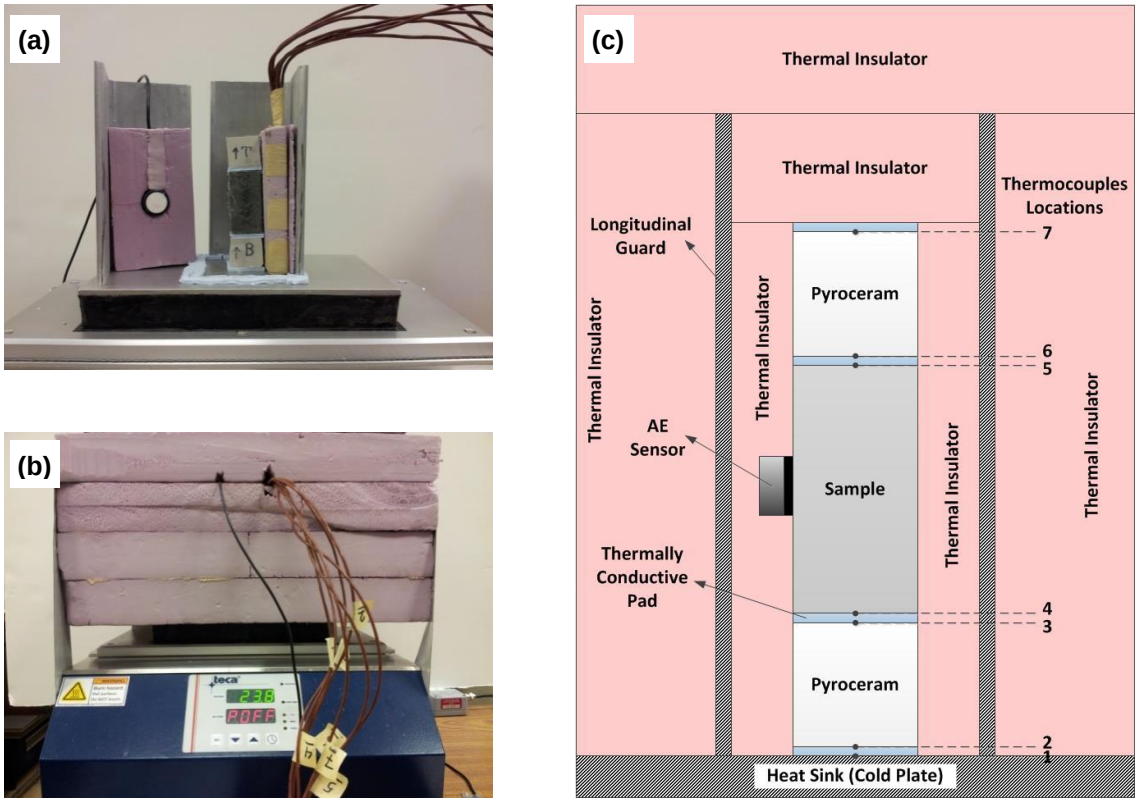

Fig. 2—Experimental setup: (a) mortar sample and Pyroceram specimens on the two stage cold plate; (b) entire experimental setup with insulation; (c) schematic of mortar sample inserted between Pyroceram material inside LGCC with AE sensor.

3.2 Acoustic Emission Measurements

Acoustic emission (AE) activity was measured during freezing and thawing. The acoustic events refer to sound waves that are produced when a material undergoes cracking, resulting in stress waves due to the energy release in a material. Acoustic waves and corresponding energy could be released by generation of cracks or microcracks under several types of internal or external loading. The detected AE can cover a wide range of inaudible and audible frequencies [31]. Therefore, a threshold value is often assigned for frequencies or amplitudes to filter environmental noise. Piezoelectric sensors are often used to convert the captured acoustic waves into electrical signals. The strength of the signals (the amplitude and duration of the waves) generally depends on the amount of released energy, distance, and orientation of the source with respect to the sensor, and the nature of the transferring medium [31,32]. The signals are then amplified and recorded in a data acquisition system. The area under the absolute value of the surface displacement can be calculated and considered as the 'AE signal energy' that is released. This AE signal energy is proportional to the fracture energy [26,33,34].

AE can be performed in either a passive or active mode. In the passive mode, AE transducers are attached to samples to capture acoustic waves generated by the formation of cracks or microcracks during the test. These acoustic waves are then analyzed to determine the quantity and behavior of the resulting damage. In the active mode, coupled transducers are attached at a known distance from one another on the surface of the samples. One of the coupled transducers generates known pulses and the other transducers record the sent pulses. The changes in pulse properties and its speed through the sample during the experiment indicate damage occurring in the sample.

In this study, both passive and active techniques were used to measure freeze/thaw damage in mortar samples containing NaCl solution. A Vallen AMSY5[1] acoustic emission system with the capability of wave transient recording (TR) was used. Therefore, a complete waveform diagram of any captured wave could be recorded and then analyzed. VS375-M cylindrical broadband sensors with a diameter of 20.3 mm and a height of 14.3 mm were used in this study. This type of transducer is a high frequency transducer with its peak sensitivity at 375 kHz. It is ideally suited for detecting waves due to crack growth in noisy environments. During testing, the acoustic waves generated due to the crack/microcrack formation were

captured by the AE sensor and then converted to electrical signals. The electrical signals were processed and magnified by preamplifiers. AE pre-amplifiers are used to transform the high-impedance signal of a sensor to a low-impedance signal suitable for transmission through long cables. A data acquisition system with the capability of streaming TR data up to 10 MHz was used to record the results. A noise threshold of 40 dB was considered for all AE sensors to exclude surrounding environmental noise.

Before and after the freeze/thaw test, two coupled AE sensors were used to perform active AE measurement through the length of the sample. During the freeze and thaw test, one AE sensor was used to record a continuous passive AE measurement. All sensors were installed using high vacuum silicone grease (Dow Corning[1]) containing polydimethylsiloxane, amorphous silica, dimethyl siloxane, and hydroxyl-terminated. This grease has good resistance to water, chemicals, and high and low temperatures; and it was found to be stable over the temperature range of the test. A slight force was applied to the sensor to have a better contact at the interface between the sensors and the sample.

3.3 Temperature Used for Freeze-Thaw Testing

In this study, each mortar sample was exposed to one freeze/thaw cycle in order to determine freezing and thawing temperatures of solution in mortar samples by using the two stage cold plate. Samples saturated with different concentrations of NaCl solution (up to 26 % by mass) were tested. Temperature was controlled to vary from 24 °C to -40 °C. Fig. 3 shows the temperature of the cold plate for this test. The initial temperature of the test was set to remain at 24 °C for one hour to allow the sample to equilibrate. After the initial temperature became stable, the bottom surface was cooled by controlling the temperature of the cold plate. The cold plate was cooled at a rate of 2 °C/h within 32 h. At -40 °C, the temperature was kept constant for 4 h to allow the sample to again reach equilibrium. Then, the temperature was increased to 24 °C at a rate of 4 °C/h within 16 h. It should be noted that other temperatures and conditions can be applied for freezing and thawing tests.

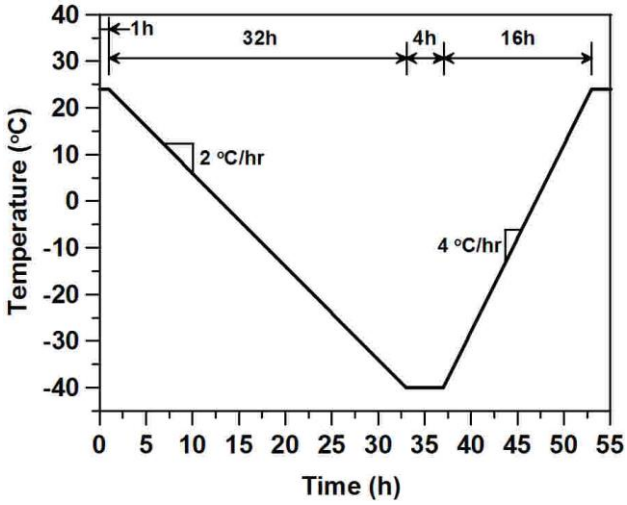

Fig. 3—Temperature of cold plate used for freeze/thaw testing.

4.0 Results and Discussion

4.1 Temperature and Heat Flow during Cooling and Heating

Heat flow is the rate of energy (i.e., heat) passing through a sample due to a temperature gradient. At steady state, the temperature gradients along the sections can be calculated from temperatures measured at the top and bottom of the two Pyroceram meter bars and the sample. Heat flow can also be calculated by knowing the thermal conductivity of Pyroceram, Eq. 1. All calculations are done in accordance with ASTM E1225-09 [15], D5470-12 [28], and C1045-07 [35]. It should be noted that these calculations are for steady state conditions, while the current experimental program was performed in a quasi-steady state condition, since the temperature of the mortar sample was decreased or increased gradually. To reach almost steady state conditions, the heating and cooling rates were assigned to be relatively low. Heat flow per unit area for the top and bottom Pyroceram meter bars can be calculated by Eq. 2 and Eq. 3 as follows:

$$q_T = \lambda_{PC}.\frac{T_6 - T_7}{d_{PC}} \quad (2)$$

$$q_B = \lambda_{PC}.\frac{T_2 - T_3}{d_{PC}} \quad (3)$$

where:

q_T = *Heat flow per unit area (W/m²) through top Pyroceram meter bar at (T_6+T_7)/2 when the sample temperature is at T_{ave},*

q_B = *Heat flow per unit area (W/m²) through bottom Pyroceram meter bar at (T_2+T_3)/2 when the sample temperature is at T_{ave},*

λ_{PC} = *Thermal Conductivity (W/(m·K)) of Pyroceram at its average temperature calculated by Eq. 1 [29],*

d_{PC} = *Thickness of Pyroceram meter bar (m),*

T_i = *Temperature (°C) measured by thermocouple at location i (see Fig. 2), and*

$T_{ave} = (T_5 + T_4)/2$.

After calculating the heat flow per unit area through the top and bottom Pyroceram meter bars, the heat flow through the mortar sample can be calculated by Eq. 4 and Eq. 5:

$$q_{Sample} = \frac{q_T + q_B}{2} \quad (4)$$

$$Q_{Sample} = q_{Sample}.A \quad (5)$$

where:

q_{sample} = *Average heat flow per unit area (W/m²) through mortar sample at T_{ave},*

Q_{sample} = *Average heat flow (W) through mortar sample at T_{ave}, and*

A = Cross-sectional area of the sample (m²).

In addition, ΔQ_{sample}, the heat flow that is consumed or released by the mortar sample at T_{ave} (i.e., heat flow inward or outward sample) can be estimated by Eq. 6:

$$\Delta Q_{Sample} = (q_B - q_T).A \quad (6)$$

Fig. 4 shows the temperatures of the sample and Pyroceram meter bars at seven different locations (as indicated in Fig. 2c). Heat flows (i.e., ΔQ_{Sample} and Q_{Sample}) were also calculated and shown in Fig. 4 and Fig. 5 for one dry sample and for wet samples containing 0 %, 5 %, or 23.3 % by mass NaCl solution. For samples containing solutions with NaCl concentrations less than or equal to 10 %, a single exothermic peak was observed during cooling that corresponds to the freezing point of pore solution (containing NaCl). However, for samples containing solutions with NaCl concentration greater than 10 %, two exothermic peaks were observed during cooling. The first exothermic peak became larger with increasing salt concentration. The second exothermic peak occurred gradually and it was therefore difficult to determine its exact onset time.

During the heating process, one endothermic peak was observed for all concentrations of NaCl solution. This peak corresponds to the thawing of ice in contact with the pore solution. No peaks were detected for the dry sample during cooling or heating, indicating that no heat was released or absorbed due to solid/liquid phase changes, as would be expected. The difference between cooling and heating processes for heat flow versus temperature curves (Fig. 5) can be attributed to the difference in cooling and heating rates, and the quasi-steady-state nature of heat flow in the experimental setup.

It should be noted that a temperature rise was observed at exothermic peaks. The temperature increase was created by the large transfer of latent heat to the surrounding environment (meter bars and thermocouples). Such a temperature rise at the freezing point is often seen when larger samples are frozen in low temperature calorimetry experiments [8,36]. A similar phenomenon was detected during thawing at which temperature remained constant for a short period of time due to the melting phase change absorbing energy.

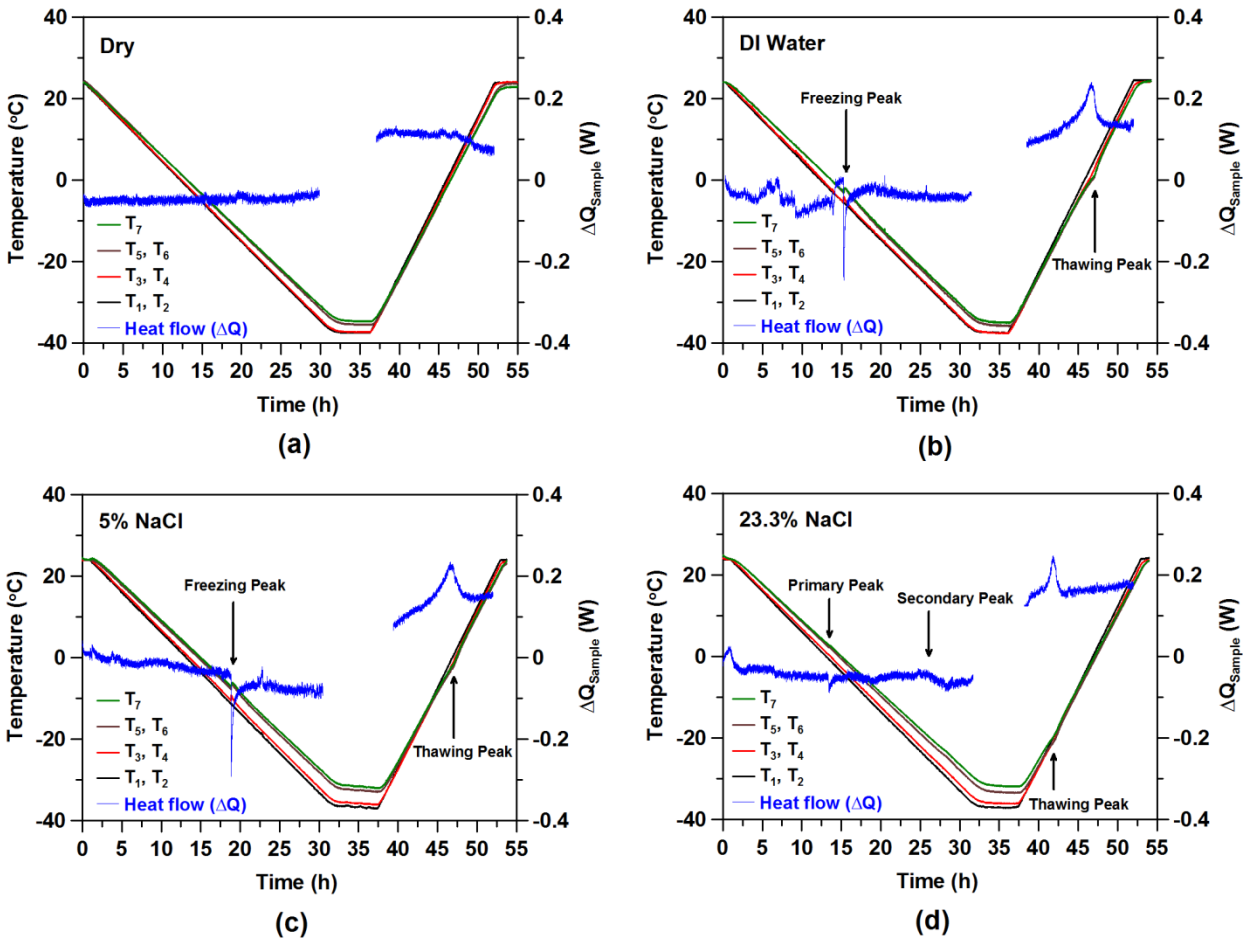

Fig. 4— Temperatures of sample and Pyroceram meter bars at different locations together with corresponding consumed/released heat flow (ΔQ_{Sample}) versus time for (a) dry sample; (b) sample saturated with deionized water; (c) sample saturated with 5 % NaCl solution; and, (d) sample saturated with 23.3 % NaCl solution.

The slope of heat flow versus temperature increases with an increase of the salt concentration (Fig. 5). This means that the heat flow is more sensitive to the temperature change for samples saturated with a greater concentrated NaCl solution.

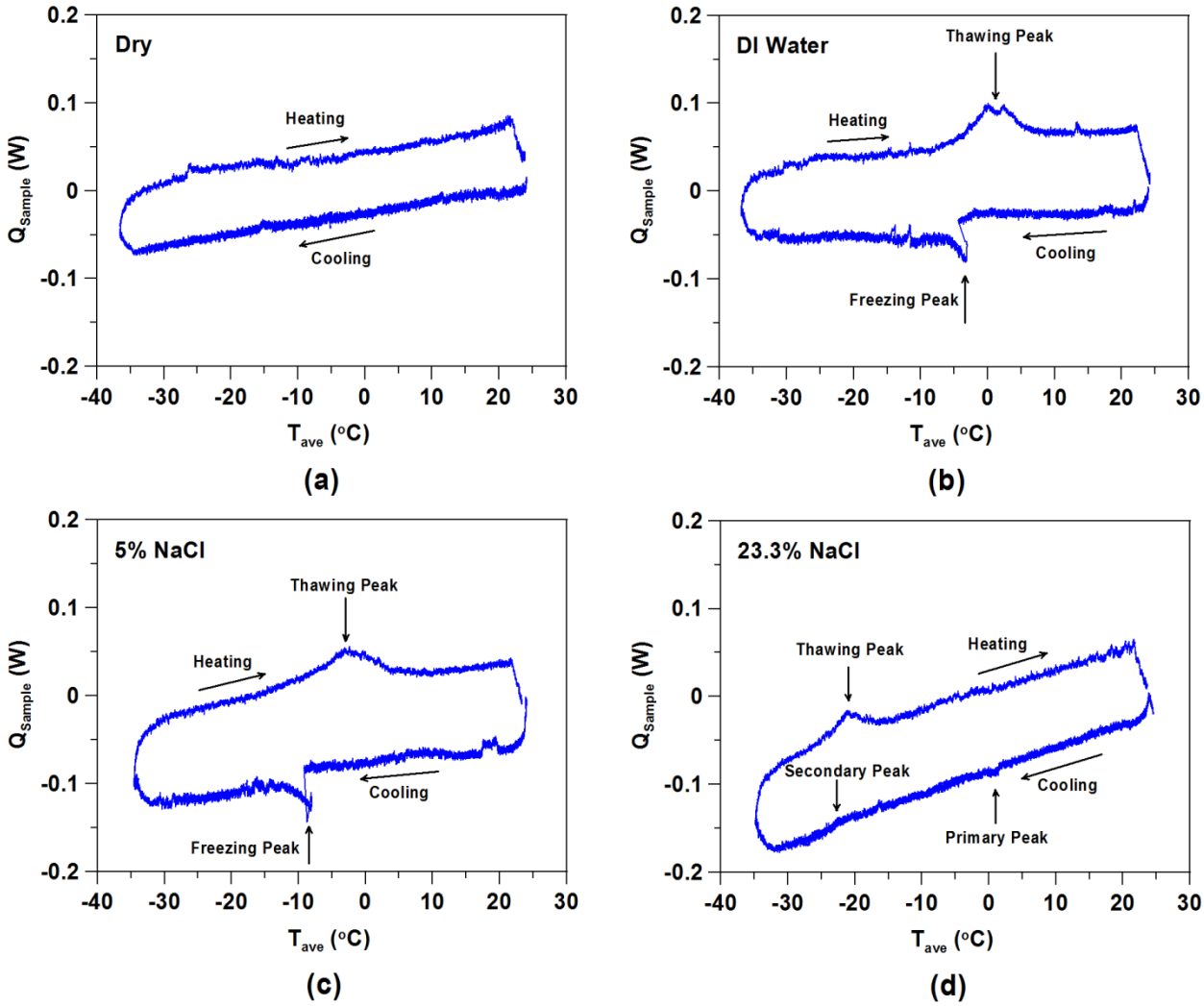

Fig. 5—Heat flow through sample (Q_{Sample}) versus average temperature for (a) dry sample; (b) sample saturated with deionized water; (c) sample saturated with 5 % NaCl solution; and, (d) sample saturated with 23.3 % NaCl solution.

4.2 Freeze and Thaw Temperatures

Water and salt solutions may freeze at a temperature below their freezing point. This phenomenon is known as super-cooling or under-cooling. In general, a liquid below its freezing point crystallizes only in the presence of a seed crystal or nucleus. However, lacking any such seeds or nuclei or presence of any inhibitor forces, the liquid phase can be maintained down to the temperature at which homogeneous crystal nucleation occurs [37]. In the opposite case, a solid will almost always melt at its melting

temperature (i.e., it cannot be “superheated”). For this reason, it is the melting point which is usually utilized to identify the liquidus line in a phase diagram [38].

NaCl-rich solution in the pores of the mortar sample could freeze at a lower temperature than expected from the NaCl solution phase diagram, but should thaw at the same liquidus temperature as indicated on the phase diagram. Indeed, under-cooling action was observed during the cooling process for mortar samples saturated with NaCl solutions. Freezing and thawing points for samples saturated with solution of different dosages of NaCl salt are indicated in Fig. 6; they are also compared to freezing and thawing points for a bulk NaCl solution derived from the NaCl-H_2O phase diagram. Since the heat flowed downwards during cooling, the pore solution is likely to have frozen first at the bottom, propagating upward. Therefore, the freezing point at the bottom of the sample may be more representative of the actual freezing point of the sample.

While the freezing points at the bottom and the top of the mortar samples were observed to be different, their thawing points were quite similar. For samples containing solutions with a NaCl concentration of more than 13 %, two freezing points were reported in Fig. 6 corresponding to the two exothermic events observed during cooling. For samples containing solution with NaCl concentration less than or equal to 8 %, the point of the single observed exothermic event was considered as the first freezing point, while for the sample with a solution of 10 % NaCl concentration, the single observed exothermic event was reported as the second freezing point. This was done for consistency with the general trend for freezing points versus NaCl concentration. For 10 % NaCl concentration, the first exothermic point might not have been detected due to a very small heat release (small freezing event).

The second freezing point for high concentrations could be attributed to formation of ice in the pore structure, while the origin of the first freezing point is unknown, as its temperature is above the NaCl solution liquidus line. The possible explanations for this exothermic behavior could be 1) the formation of $NaCl{\cdot}2H_2O$ at concentrations less than the expected eutectic concentration due to confinement, capillary pressure, and surface interaction within the pore structure; 2) the generation of an alternative phase change due to the composition of pore solution and chloride binding; 3) the inhomogeneous distribution of

NaCl within the specimen microstructure during the saturation process or, 4) the formation of NaCl salt on the pore structure surface.

Table 3 shows the freezing and thawing temperatures of the top and bottom surfaces of the samples as well as the amount of under-cooling with respect to the liquidus line. For high concentrations, the second freezing point was used to calculate the amount of under-cooling, as it may be a better representative of ice formation. For samples with solution concentrations between 5 % and 8 % NaCl, an increase in freezing temperature was observed which can be followed by the first freezing points observed for concentrations greater than 10 % NaCl. In addition, for samples saturated with highly concentrated NaCl solutions, less depression (under-cooling) was observed compared to samples saturated with low concentration solutions. This can be attributed to the reduction of pore solution concentration due to the early phase change at the first freezing point. Further research is needed to understand the observed phenomenon at the first freezing point.

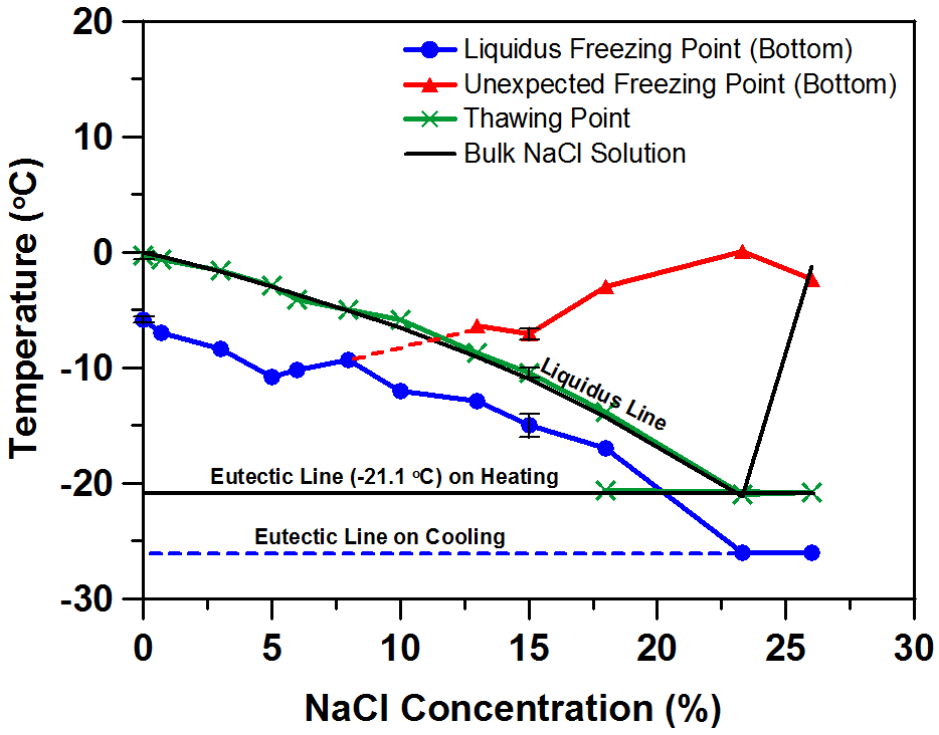

Fig. 6— Freezing and thawing points of samples saturated with different NaCl solutions compared to the freezing points of bulk NaCl solution.

Table 3— Freezing and thawing points at the bottom and top surfaces of samples (°C).

NaCl solution concentration (%)	Freezing point of bulk NaCl solution	Freezing point				Thawing point		Amount of under-cooling w.r.t. liquidus line[+]
		First peak		Second peak				
		Bottom	Top	Bottom	Top	Bottom	Top	
0 (Dry)	-	-	-	-	-	-	-	-
0 (DI Water)	0.0	-6.1	-3.8	-	-	0.3	0.0	-6.1
0.7	-0.4	-7.0	-5.2	-	-	-0.1	-0.6	-6.7
3	-1.6	-8.3	-6.5	-	-	-1.1	-1.6	-6.7
5	-3.0	-10.8	-7.9	-	-	-2.3	-2.9	-7.8
6	-3.7	-10.2	-6.9	-	-	-3.9	-4.1	-6.6
8	-5.1	-9.3	-6.7	-	-	-4.8	-5.0	-4.2
10	-6.5	-	-	-12.0*	-9.3*	-5.3	-5.8	-5.5
13	-9.1	-6.4	-4.2	-12.9**	-10.6**	-8.1	-8.7	-3.8
15	-10.9	-6.1	-5.3	-15.5**	-13.0**	-10.1	-10.9	-4.5
18	-14.3	-3.0	-1.3	-17.0**	-15.0**	-15.0[#]	-15.5[#]	-2.7
23.3	-21.1	0.1	2.1	-26.0**	-23.5**	-20.7	-21.0	-4.9
26	-21.1[++]	-2.4	-0.8	-26.0**	-23.5**	-20.6	-20.8	-4.9

* For samples containing 10 % NaCl solution, one peak was observed and considered as the second freezing point. It was assumed that the first freezing point was not large enough to detect.

** For these concentrations, approximate values are reported since it was difficult to find the exact onset value for heat transfer.

[+] To calculate the amount of under-cooling, the lowest freezing point is subtracted from the freezing point of the corresponding bulk NaCl solution.

[++] For this dosage, there are two freezing points according to the aqueous NaCl phase diagram (Fig. 1). Here, the second freezing point is reported as it corresponds to the ice formation.

[#] For this concentration, two thawing points were observed (Fig. 6). The one which is reported in this table corresponds to the liquidus line. The other melting point was observed around -20.6 °C which corresponds to the eutectic temperature.

4.3 Passive Acoustic Emission

Plots of AE event amplitude versus temperature for the dry sample and samples saturated with DI water, 5 % NaCl solution, and 15 % NaCl solution are shown in Fig. 7 during cooling and heating. For the dry sample, relatively very few AE events were recorded during cooling and heating (Fig. 7a). These acoustic events are most likely attributed to the coefficient of thermal expansion (CTE) mismatch between aggregate and paste, and they disappear in subsequent freeze and thaw cycles [1]. A greater number of AE events were observed for the solution-saturated samples during freezing. While the saturated samples had AE activities associated with the CTE mismatch, greater levels of AE activity were detected

due to the damage and cracking caused by freezing and thawing. It should be noted that the amount of damage varies with the concentration of NaCl solution.

For samples saturated with NaCl concentrations lower than 3 %, a cluster of AE activity was recorded during freezing due to crack formation generated by ice formation and osmotic pressure. Another cluster was observed during thawing (Fig. 7b) which may be attributed to additional crack formation due to osmotic pressure or crack closing. When the NaCl concentrations increased from 3 % to 8 %, the AE events during thawing diminished (Fig. 7c). For solutions with higher concentrations of NaCl, in addition to AE events due to freezing damage, the AE activity was also observed between the first and the second exothermic freezing temperatures. Moreover, a cluster of AE events was detected around -21.1 °C (the eutectic point) during heating, which corresponds to the phase transformation (melting) of $NaCl{\cdot}2H_2O$ (Fig. 7d).

For samples saturated with solutions of (0, 3, 5, 6, 10, 15, and 23.3) % NaCl, cumulative AE energy versus time is indicated in Fig. 8. While a dramatic increase in AE activity was observed for mortar samples containing lower concentrations of NaCl solution, the increase of AE activity for higher concentrations occurred gradually. This can also be explained by the slope of the AE cumulative energy curve versus time at the moments of ice formation. In other words, damage propagation and the generation of cracks or microcracks during cooling were more distributed for higher concentrations, while damage and crack development happened more suddenly for lower concentrations.

Fig. 9 shows the total cumulative acoustic energy recorded during one freeze/thaw cycle for samples saturated with different concentrations of NaCl solution. Two levels of high damage or AE activity (i.e., humps) can be seen. The first hump can be attributed to ice formation and osmotic pressure damage. The decrease of cumulative AE energy with the increase in NaCl solution concentration may be due to a reduction in the volume of ice formation, since the amount of a solvent (water) decreases in a solution (aqueous NaCl) with an increase in dosage of a solute (NaCl). The second hump can be attributed to damage due to the expansion of $NaCl{\cdot}2H_2O$ during melting at -21.1 °C. Further research is needed to investigate the effect of different phase changes on damage mechanisms in mortars during freezing and thawing.

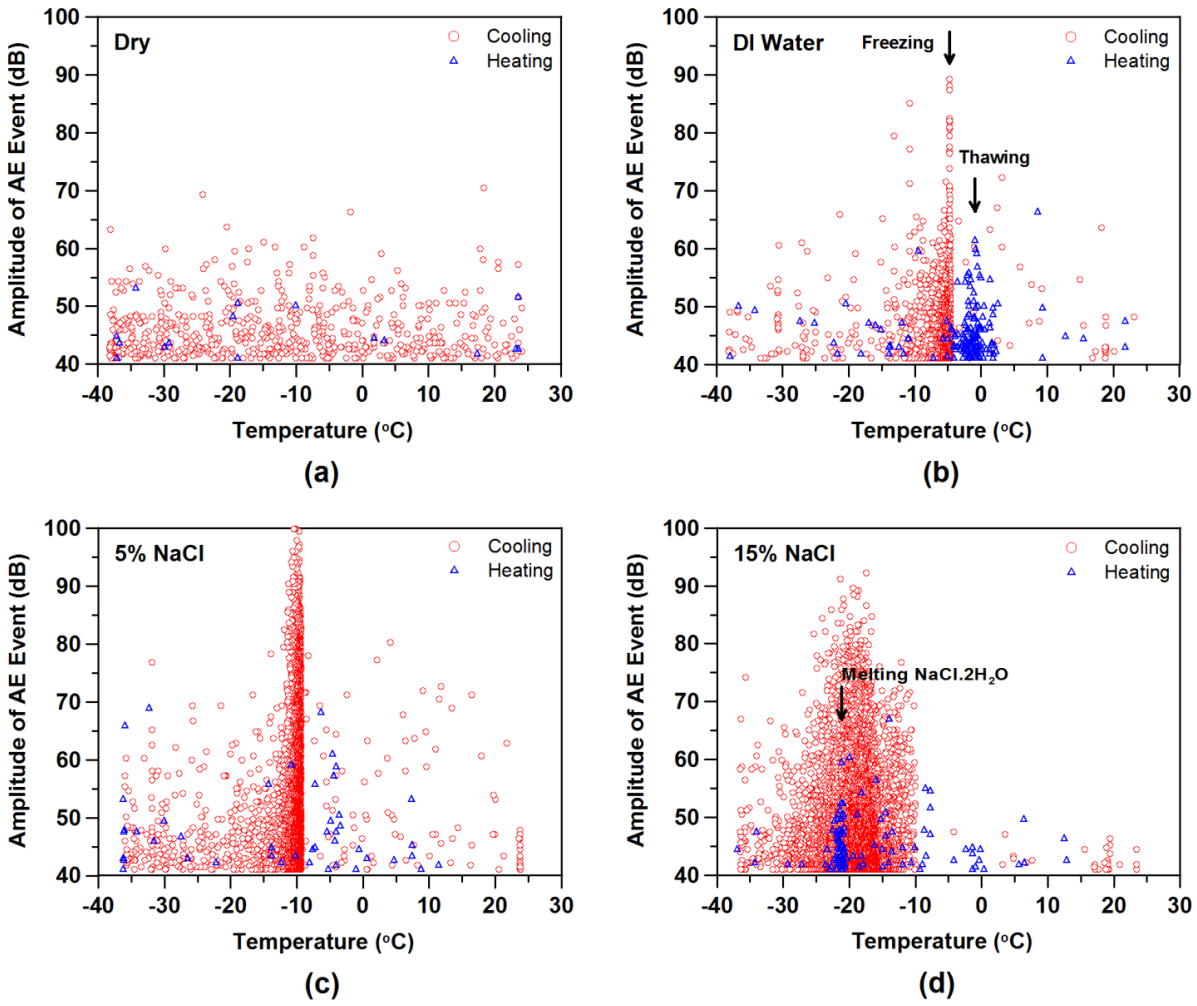

Fig. 7— Passive AE events versus temperature during cooling and heating

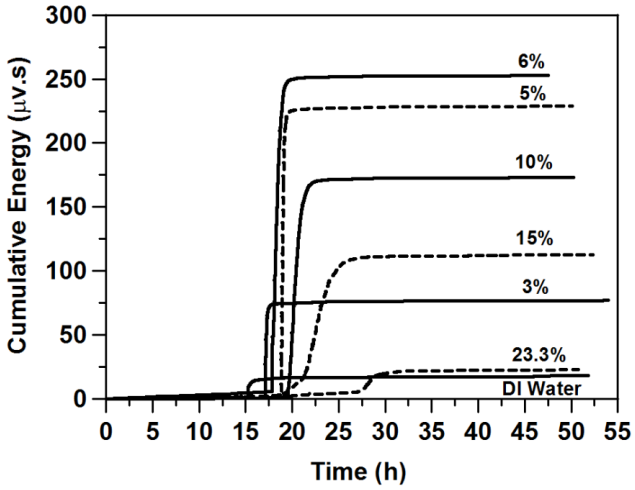

Fig. 8— Cumulative acoustic energy versus time for samples saturated with NaCl solution.

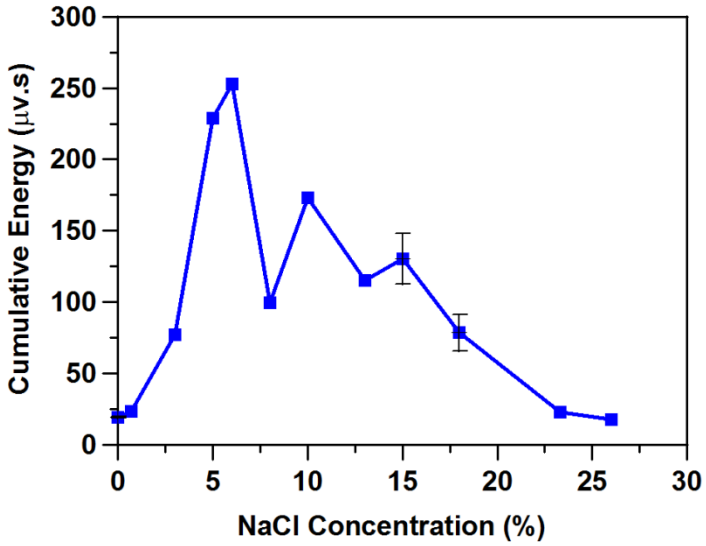

Fig. 9— Total cumulative acoustic energy due to freeze/thaw damage for samples saturated with different NaCl solutions (the error bars indicate ± one standard deviation for two replicates).

4.4 Active Acoustic Emission

The velocity of a longitudinal stress wave (*V*) can be calculated using the measured length of the sample (*L*) and the transit time (*T*) that the wave takes to pass through the length of sample (Eq. 7).

$$V = \frac{L}{T} \tag{7}$$

The velocity can be obtained for the sample before and after a freeze/thaw cycle as the sample undergoes damage. The average transmission times of four single pulses was measured along the sample in each direction. Knowing the distance between the two sensors, an average pulse velocity was calculated by the acoustic emission system in each direction. Pulse velocities were then averaged and used to calculate the relative dynamic modulus.

ASTM C597-09 [39] describes how the velocity of the longitudinal stress wave (*V*) measured in concrete can be related to the elastic properties and density of the concrete using the following relationship:

$$V = \sqrt{\frac{E(1-\mu)}{\rho(1+\mu)(1-2\mu)}} \quad (8)$$

where E, μ, and ρ are the dynamic modulus of elasticity, the dynamic Poisson's ratio, and the density, respectively.

The relative dynamic modulus E_t/E_o (the ratio of the dynamic modulus after freeze/thaw testing to the dynamic modulus before the freeze/thaw test) was used to assess the damage level of the samples as a result of freezing and thawing. It is assumed that the density and Poisson's ratio remain constant during testing. It has been shown that assuming a constant Poisson's ratio during freezing does not significantly influence the value of the dynamic modulus [20]. The damage parameter (D) is estimated using Eq. 9.

$$D = 1 - \frac{E_t}{E_o} = 1 - (\frac{V_t}{V_o})^2 \quad (9)$$

where E_o and V_o are dynamic elastic modulus and average pulse velocity, respectively, before a freeze/ thaw test; and E_t and V_t are the dynamic elastic modulus and average pulse velocity, respectively, after the freeze/thaw test.

The damage index (D) for mortar samples is shown in Fig. 10. Similar to the behavior observed for the cumulative acoustic energy, two levels of high damage (i.e., humps) can be seen. The damage that occurs at the lower concentrations of NaCl solution may be similar to what was observed during scaling tests, where more damage occurred due to a pessimism salt concentration between 3 % and 5 % NaCl [40]. Greater damage also occurred with a higher NaCl concentration solution, which appears to be caused by the combination of ice formation during freezing, the osmotic pressure, the expansion of $NaCl{\cdot}2H_2O$ during melting, and the damage caused between the first and second exothermic freezing points. The temperature at which $NaCl{\cdot}2H_2O$ melts is the eutectic temperature (-21.1 °C). At this temperature, all of the ice that has formed during freezing remains in the pores and cracks in a frozen form. As $NaCl{\cdot}2H_2O$ changes from a solid to a liquid, it expands, causing more damage in the samples.

This can be also observed in Fig. 7d as AE events were observed for melting of $NaCl \cdot 2H_2O$. In addition, another AE cluster observed for high concentration between the first and second freezing exothermic behavior (Fig. 7d) implies an additional damage mechanism happening for high concentrations. Above a concentration of 15 %, the damage parameter decreases, showing that the damage due to a combination of ice formation, osmotic pressure, $NaCl \cdot 2H_2O$ melting, and the damage caused between the first and second exothermic freezing points passes a critical combination. It should be noted that relatively lesser AE energy was measured for the concentration of 15 % (Fig. 8 and Fig. 9).

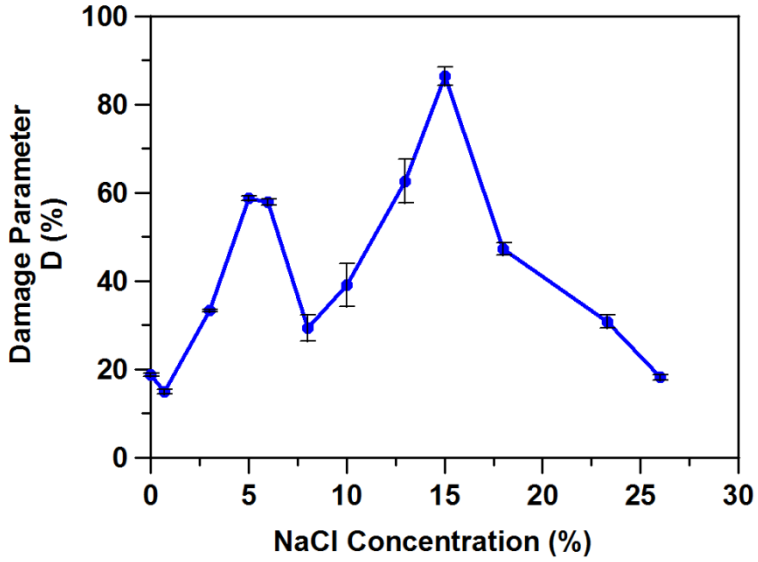

Fig. 10—Decrease of the relative dynamic elastic modulus (damage parameter) due to freeze and thaw damage for samples saturated with different dosages of NaCl solution (the error bars indicate ± one standard deviation for four replicates of pulse velocity testing).

5.0 Conclusions

In this paper, the freeze/thaw behavior of mortar samples that were saturated by solutions with various concentrations of NaCl salt was investigated. A low-temperature longitudinal guarded comparative calorimeter (LGCC) was developed and equipped with acoustic emission sensors to measure the heat flux and acoustic emission activities (i.e., damage or cracking behavior) of the mortars during freezing and thawing.

Mortar samples exhibited different exothermic behaviors during cooling (freezing) while showing only one endothermic activity during heating (melting). For lower concentrations of NaCl, one exothermic peak was observed in heat flux due to ice formation. For higher concentrations, however, two exothermic events were seen. The second exothermic peak was due to ice formation, while the cause of the first exothermic peak remains unknown and more investigation is needed to understand and validate possible causes. Heat release due to ice formation occurred at a lower temperature than what would be expected from a NaCl aqueous solution. The frozen solution which was created during cooling in mortar was observed to melt at the same temperature as would be expected for the bulk NaCl solution. A greater freezing point depression was observed for samples saturated with a lower NaCl salt concentration in comparison to samples saturated with high concentration.

Two distinctive features (i.e., humps) were observed in the cumulative energy and damage index obtained from acoustic activities. The first hump may be attributed to ice formation and the resulting osmotic pressure that cause cracking and damage. The second distinct feature (second hump) may be attributed to expansion of $NaCl \cdot 2H_2O$ during melting at its eutectic temperature (-21.1 °C), which can result in further stress and cracking. Additional damage may occur due to destructive phenomenon observed for high concentration between the first and second freezing exothermic behavior. For mortar samples saturated with 5 % and 15 % of NaCl solution, higher freeze and thaw damage was observed.

6.0 Acknowledgements

The experiments reported in this paper were conducted in the Pankow Materials Laboratory at Purdue University. The authors would like to acknowledge the support from the Joint Transportation Research Program administered by the Indiana Department of Transportation and Purdue University. The contents of this paper reflect the views of the authors, who are responsible for the facts and the accuracy of the data presented herein, and do not necessarily reflect the official views or policies of the Indiana Department of Transportation, nor do the contents constitute a standard, specification, or regulation.

7.0 References

[1] W. Li, M. Pour-Ghaz, J. Castro, J. Weiss, Water absorption and critical degree of saturation relating to freeze-thaw damage in concrete pavement joints, Journal of Materials in Civil Engineering. 24 (2012) 299–307.

[2] T.C. Powers, The air requirement of frost-resistant concrete, Highway Research Board. 29 (1949) 184–211.

[3] T. Powers, A working hypothesis for further studies of frost resistance of concrete, in: Journal of the American Concrete Institute, Portland Cement Association, Detroit, Michigan, 1945: pp. 245–272.

[4] T.C. Powers, The physical structure and engineering properties of concrete, Research Department Bulletin, Portland Cement Association. 90 (1958) 27 pages.

[5] J. Beaudoin, C. MacInnis, The mechanism of frost damage in hardened cement paste, Cement and Concrete Research. 4 (1974) 139–147.

[6] G. Litvan, Frost action in cement in the presence of de-icers, Cement and Concrete Research. 6 (1976) 351–356.

[7] G. Scherer, Crystallization in pores, Cement and Concrete Research. 29 (1999) 1347–1358.

[8] J. Kaufmann, Experimental identification of damage mechanisms in cementitious porous materials on phase transition of pore solution under deicing salt attack, École polytechnique fédérale de Lausanne (EPFL), 2000.

[9] P.K. Mehta, P.J. Monteiro, Concrete: microstructure, properties, and materials, Third, McGraw-Hill, New York, 2005.

[10] R. Beddoe, M. Setzer, A low-temperature DSC investigation of hardened cement paste subjected to chloride action, Cement and Concrete Research. 18 (1988) 249–256.

[11] B. Han, J.H. Choi, J. Dantzig, J.C. Bischof, A quantitative analysis on latent heat of an aqueous binary mixture, Cryobiology. 52 (2006) 146–51.

[12] R. Beddoe, M. Setzer, Phase transformations of water in hardened cement paste, a low-temperature DSC investigation, Cement and Concrete Research. 20 (1990) 236–242.

[13] B. Johannesson, Dimensional and ice content changes of hardened concrete at different freezing and thawing temperatures, Cement and Concrete Composites. 32 (2010) 73–83.

[14] S. Jacobsen, E. Sellevold, S. Matala, Frost durability of high strength concrete: Effect of internal cracking on ice formation, Cement and Concrete Research. 26 (1996) 919–931.

[15] ASTM E1225- Standard test method for thermal conductivity of solids by means of the guarded-comparative-longitudinal heat flow technique, ASTM International, West Conshohocken, PA, 2009.

[16] D.-J. Yoon, W.J. Weiss, S.P. Shah, Detecting the extent of corrosion with acoustic emission, Transportation Research Record. (2000) 54–60.

[17] D.-J. Yoon, W.J. Weiss, S.P. Shah, Assessing damage in corroded reinforced concrete using acoustic emission, Journal of Engineering Mechanics. 126 (2000) 273–283.

[18] M. Pour-Ghaz, J. Weiss, Quantifying damage due to aggregate expansion in cement matrix, Advances in the Material Science of Concrete. 270 (2010) 101–114.

[19] S. Puri, J. Weiss, Assessment of localized damage in concrete under compression using acoustic emission, Journal of Materials in Civil Engineering. 18 (2006) 325–333.

[20] Z. Yang, W.J. Weiss, J. Olek, Water transport in concrete damaged by tensile loading and freeze–thaw cycling, Journal of Materials in Civil Engineering. 18 (2006) 424–434.

[21] W.S. Park, J.H. Lee, Evaluation of freeze-thaw damage in concrete by one-sided stress wave velocity measurement technique, Key Engineering Materials. 270-273 (2004) 1604–1609.

[22] M. Ohtsu, Nondestructive evaluation of damaged concrete due to freezing and thawing by elastic-wave method, Journal of Advanced Concrete Technology. 3 (2005) 333–341.

[23] W. Li, W. Sun, J. Jiang, Damage of concrete experiencing flexural fatigue load and closed freeze/thaw cycles simultaneously, Construction and Building Materials. 25 (2011) 2604–2610.

[24] M.A. Taylor, Passive acoustic emission for quantitative evaluation of freeze thaw and alkali aggregate reaction in concretes, in: F. Ansari, S. Sture (Eds.), Nondestructive Testing of Concrete Elements and Structures, New York, NY, 1992: pp. 1–12.

[25] Y. Qian, Y. Farnam, J. Weiss, Using acoustic emission to quantify freeze-thaw damage of mortar saturated with NaCl solutions, in: T. Miyagawa (Ed.), International Conference on Sustainable Construction Materials & Technologies, Kyoto, Japan, 2013: pp. 1–10.

[26] H. Shimada, K. Sakai, G.G. Litvan, Acoustic emissions of mortar subjected to freezing and thawing, in: Second International Conference on Durability of Concrete, Montreal, Canada, 1991: pp. 263–278.

[27] ASTM C305 - Standard practice for mechanical mixing of hydraulic cement pastes and mortars of plastic consistency, ASTM International, West Conshohocken, PA, 2012.

[28] ASTM D5470- Standard test method for thermal transmission properties of thermally conductive electrical insulation materials, ASTM International, West Conshohocken, PA, 2012.

[29] Thermal properties of pyroceram code 9606, Private Communication from the National Institute of Standards and Technology (NIST), Gaithersburg, MD.

[30] www.teca-eu.com, Low temperature cold plate - CPV Cascade CCP-22, (2012) 1–2.

[31] M. Pour-ghaz, R. Spragg, J. Castro, J. Weiss, Can acoustic emission be used to detect alkali silica reaction earlier than length change?, in: 14th International Conference on Alkali-Aggregate Reaction, University of Texas; Austin, Texas, 2012: pp. 1–10.

[32] H. Vallen, AE testing fundamentals, equipment, applications, Nondestructive Testing. 7 (2002).

[33] E.N. Landis, L. Baillon, Experiments to relate acoustic emission energy to fracture energy of concrete, Journal of Engineering Mechanics. 128 (2002) 698–702.

[34] M. Pour-Ghaz, Detecting damage in concrete using electrical methods and assessing moisture movement in cracked concrete, Purdue University, 2011.

[35] ASTM C1045- Standard practice for calculating thermal transmission properties under steady-state conditions, ASTM International, West Conshohocken, PA, 2007.

[36] S. Jacobsen, D. Sœther, E. Sellevold, Frost testing of high strength concrete: Frost/salt scaling at different cooling rates, Materials and Structures. 30 (1997) 33–42.

[37] P.G. Debenedetti, H.E. Stanley, Supercooled and glassy water, Physics Today. 56 (2003) 40–46.

[38] J.A. Ramsay, A new method of freezing-point determination for small quantities, The Journal of Experimental Biology. 26 (1949) 57–64.

[39] ASTM C597- Standard test method for pulse velocity through concrete, ASTM International, West Conshohocken, PA, 2009.

[40] John Valenza, Mechanism for salt scaling, Princeton University, 2005.